

Mark-Recapture with Multiple Non-invasive Marks

Simon Bonner and Jason Holmberg

November 2, 2018

Abstract

1
2 Non-invasive marks, including pigmentation patterns, acquired scars, and
3 genetic markers, are often used to identify individuals in mark-recapture exper-
4 iments. If animals in a population can be identified from multiple, non-invasive
5 marks then some individuals may be counted twice in the observed data. An-
6 alyzing the observed histories without accounting for these errors will provide
7 incorrect inference about the population dynamics. Previous approaches to
8 this problem include modeling data from only one mark and combining esti-
9 mators obtained from each mark separately assuming that they are indepen-
10 dent. Motivated by the analysis of data from the ECOCEAN online whale
11 shark (*Rhincodon typus*) catalog, we describe a Bayesian method to analyze
12 data from multiple, non-invasive marks that is based on the latent-multinomial
13 model of Link et al. (2010). Further to this, we describe a simplification of the
14 Markov chain Monte Carlo algorithm of Link et al. (2010) that leads to more
15 efficient computation. We present results from the analysis of the ECOCEAN
16 whale shark data and from simulation studies comparing our method with the
17 previous approaches.

18 **Keywords:** Latent multinomial model; Mark-recapture; Multiple marks; Non-invasive
19 marks; Photo-identification; Whale sharks

20 **1 Introduction**

21 Non-invasive marks (also called natural marks) include patterns in pigmentation,
22 genetic markers, acquired scars, or other natural characteristics that allow researchers
23 to identify individuals in a population without physical capture. Visible marks have
24 long been used to identify individuals of some species that are hard to tag, particularly
25 marine mammals, and non-invasive marks are now being used more widely. Yoshizaki
26 et al. (2009) and Yoshizaki et al. (2011) reference studies including:

- 27 • studies based on photographs of large cats (cheetahs, snow leopards, and tigers),
- 28 • scar patterns on marine mammals (manatees and whales),
- 29 • skin patterns of reptiles and amphibians (snakes, crocodiles, and salamanders),
- 30 • and genetic marks in various species (bears, wombats, and whales).

31 The primary advantage of non-invasive marks over man-made marks is that they can
32 often be observed from a distance or through the collection of secondary material
33 (e.g. hair samples or scat). This means that individuals can be identified passively
34 without physical contact. Further, many non-invasive marks allow every individual
35 in the population to be identified from birth. However, mark-recapture data collected
36 from non-invasive marks can present several modeling challenges. Previous statistical
37 developments have considered that non-invasive marks may be misidentified at non-
38 negligible rates (Lukacs and Burnham, 2005; Wright et al., 2009; Yoshizaki et al.,
39 2011), that individuals' marks may change over time (Yoshizaki et al., 2009), and
40 that some non-invasive marks (e.g scar patterns) may be restricted to a subset of the
41 population (Da-Silva et al., 2003; Da-Silva, 2006). We consider the problem of mod-
42 eling the demographics of a population from mark-recapture data when individuals
43 have been identified from multiple, non-invasive marks.

44 The specific application we consider concerns modeling the aggregation of whale
45 sharks (*Rhincodon typus*) in Ningaloo Marine Park (NMP), off the west coast of
46 Australia. Whale sharks aggregate at NMP each year between April and July. During
47 this time, whale sharks are located by tour companies and photographs are taken by
48 tourists and tour operators who upload their images to the online ECOCEAN whale
49 shark library. Whale sharks can be identified by the unique pattern of spots on their
50 flanks, and computer assisted methods are used to match photographs in the library.
51 Matches are then used to generate capture histories which provide information about
52 the timing of the sharks' arrival and departure from NMP and their survival across
53 years (see Holmberg et al., 2009, for further details).

54 The challenge in modeling this data is that sharks may be photographed from
55 either the left or the right side, but the spot patterns are not the same. This means
56 that photographs from the two sides of a shark cannot be matched without further in-
57 formation. In particular, the spot patterns on the right and left can only be matched
58 if the shark was photographed from both sides during one encounter or more. If this
59 has not happened then photographs of the same shark taken from different sides on
60 different occasions cannot be linked and the shark will contribute two separate histo-
61 ries to the observed data. Ignoring this problem and naively modeling the observed
62 encounter histories will inflate the apparent number of sharks identified and create
63 dependence between the encounter histories. This violates a key assumption of most
64 mark-recapture models. One solution is to construct encounter histories based on
65 photographs from either the left or right side alone, but this removes information
66 from the data. As an alternative, Wilson et al. (1999, pg. 294) suggests combining
67 inferences obtained from left- and right-side photographs of bottlenose dolphins by av-
68 eraging separate point estimates and computing standard errors assuming that these
69 estimates are independent. The bias of the combined estimate is the average of the

70 biases of the individual estimates (the combined estimate is unbiased if the individual
71 estimates are unbiased), but the assumption of independence is violated and standard
72 errors will be underestimated. More recently, Madon et al. (2011) describes a method
73 to estimate abundance from multiple marks by adjusting the sufficient statistics re-
74 quired to compute the Jolly-Seber estimator, but we have concerns with this method.
75 Though the observed counts underestimate some of the statistics and overestimate
76 others, Madon et al. (2011) uses the same adjustment factor for all and constrains its
77 value to be between 0 and 1. Simulations Madon et al. (2011) presents indicate a clear
78 problem in that the coverage of confidence intervals is much lower than their nominal
79 value, even when the population is large and the capture probability is close to 1.
80 These issues are discussed further in Bonner (2013). We are also aware of methods
81 similar to ours being developed concurrently by McClintock et al. (2013).

82 The primary contribution of our work is to provide a valid method of modeling
83 a population's dynamics using data from multiple, non-invasive marks. We do so
84 by constructing an explicit model of the observation process that allows for multiple
85 marks and applying Bayesian methods of inference via Markov chain Monte Carlo
86 (MCMC) sampling. Our model is a modification of the latent multinomial model
87 (LMM) presented in Link et al. (2010) for modeling mark-recapture data based on
88 genetic marks with non-negligible misidentification rates. Further to this, we provide
89 a more efficient simplification of the MCMC algorithm of Link et al. (2010).

90 **2 Data**

91 Data for our analysis were obtained from the ECOCEAN on-line whale shark li-
92 brary (available at www.whaleshark.org). This library contains photographs of
93 whale sharks taken by recreational divers and tour operators worldwide and sub-

94 mitted electronically. The library has been operational since 2003, and more than
95 41,000 photographs had been submitted by over 3,300 contributors as of January,
96 2013.

97 New photographs submitted to the library are matched against existing pho-
98 tographs using two computer algorithms (Arzoumanian et al., 2005; Van Tienhoven
99 et al., 2007). Identities are based on the pattern of spots on the flank, believed
100 to be unique, and the algorithms operate independently using significantly different
101 approaches to provide complementary coverage in evaluating matches. All matches
102 generated by the computer algorithms are confirmed by two or more trained research
103 staff to minimize the probability of false matches. Further details on the study site,
104 the observation protocols, and the algorithms for matching photographs are provided
105 in Holmberg et al. (2009).

106 We model only the data collected from the northern ecotourism zone of NMP
107 during the 16 week period between April 1 and July 31, 2008. This period was divided
108 into 8 capture occasions of 2 weeks each, and sharks may have been encountered
109 multiple times during a single capture occasion. Five possible events may occur; on
110 each occasion, a shark may:

- 111 1) not be encountered at all (event 0)
- 112 2) be photographed from the left only (event L),
- 113 3) be photographed from the right only (event R),
- 114 4) be photographed from both sides simultaneously on at least one encounter (event
115 S), or
- 116 5) be photographed from both sides but never simultaneously (event B).

117 We will denote a generic encounter history made from these events by ω .

118 Problems with identification arise because the pattern of spots on the left and
 119 right flanks are not the same. It is only possible to match the skin patterns from the
 120 two sides of a shark if photographs of both sides were taken simultaneously during
 121 at least one capture occasion – i.e., there is at least one S in its encounter history.
 122 Otherwise, an individual photographed from both sides will contribute two encounter
 123 histories to the data set – one containing the observations of its right side and the
 124 other containing the observations of its left side.

125 Suppose, for example, that an individual’s true encounter history is 00L0B0R0.
 126 This history is not observable because the two sides of the individual were never
 127 photographed simultaneously. Hence, the individual will contribute two observed
 128 histories to the data – 00L0L000 and 0000R0R0. Working backward, the observed
 129 histories 00L0L000 and 0000R0R0 may either come from one individual encountered
 130 on three occasions or from two separate individuals each encountered on two two or
 131 more occasions.

132 For a study with T capture occasions there are $5^T - 1$ possible true capture histories
 133 (we condition on capture and ignore the zero history). Of these, $(5^T - 1) - (4^T -$
 134 $1) + 2(2^T - 1)$ histories can be observed. These include the $(5^T - 1) - (4^T - 1)$ that
 135 contain at least one S , which we call simultaneous histories, the $2^T - 1$ histories that
 136 include only 0 and L , left-only histories, and the $2^T - 1$ histories that include only
 137 0 and R , right-only histories. The remaining $(4^T - 1) - 2(2^T - 1)$ contain either L
 138 and R together and/or B but no S and cannot be observed. Individuals with these
 139 true histories contribute two observed histories to the data. When a left-only and
 140 right-only history, call them ω_L and ω_R , combine to form a third history, ω_C , we say
 141 that ω_L and ω_R are the left and right parents of child ω_C .

142 **3 Methods**

143 **3.1 Latent Multinomial Model**

144 To account for uncertainty in the true encounter histories caused by multiple marks,
145 we adapt the LMM model of Link et al. (2010). Suppose that individuals in the
146 population can have one of K possible true histories which produce a total of $L \leq K$
147 possible observable histories. The genetic misidentification model of Link et al. (2010),
148 for example, allows for three events on each capture occasion: individuals may be
149 captured and identified correctly (1), captured and misidentified (2), or not captured
150 (0). This produces $K = 3^T$ possible true histories but only $L = 2^T - 1$ observable
151 histories. Following Link et al. (2010), we define \mathbf{f} to be the L -vector of observed
152 counts for the observable histories and \mathbf{x} the latent K -vector of counts for the possible
153 true histories. The LMM is based on two assumptions about these vectors. First,
154 it assumes that each element of \mathbf{f} is a known linear combination of the elements of
155 \mathbf{x} . That is, there is a known $K \times L$ matrix \mathbf{A} such that $\mathbf{f} = \mathbf{A}'\mathbf{x}$. This limits the
156 possible values of \mathbf{x} given the observed value of \mathbf{f} , so we refer to it as the latent vector
157 constraint. Second, the LMM assumes that \mathbf{x} follows a multinomial distribution

$$\mathbf{x} \sim \text{Multinomial}(N, \boldsymbol{\pi}(\boldsymbol{\theta}))$$

158 with $N = \sum_{k=1}^K \mathbf{x}_k$ representing either the population or sample size (depending
159 on whether the model conditions on first capture) and $\boldsymbol{\pi}(\boldsymbol{\theta})$, the cell probabilities
160 dependent on parameter $\boldsymbol{\theta}$.

161 The specific model of \mathbf{x} we have fit is an extension of the Link-Barker-Jolly-Seber
162 (LBJS) model from Link and Barker (2005) modified to allow for multiple marks. We
163 are primarily interested in the arrival and departure times of the sharks at NMP and

164 so we condition on individuals being captured at least one time and ignore the zero
 165 history. In this case, N is the total number of individuals captured during the study.
 166 Note that unlike standard mark-recapture experiments the true value of N cannot be
 167 observed.

168 The key assumptions of our model are that all emigration from NMP is perma-
 169 nent, that the probability of remaining at NMP from one occasion to the next does
 170 not depend on how long an individual has been present (or any other factors), that
 171 encounters are independent between individuals and over time, that there are no
 172 losses on capture, and that the conditional probabilities of the events L , R , S , and B
 173 are constant. Under these conditions, the cell probability assigned to history ω is:

$$\pi_{\omega}(\boldsymbol{\theta}) = \xi(a|\boldsymbol{\gamma}, \boldsymbol{\phi}, \boldsymbol{p}) \cdot \rho_{\omega_a} \prod_{t=a+1}^b [\phi_{t-1}(p_t \rho_{\omega_t})^{I(\omega_t \neq 0)} (1 - p_t)^{I(\omega_t = 0)}] \cdot \chi(b|\boldsymbol{\phi}, \boldsymbol{p})$$

174 where $a = \min\{t : \omega_t > 0\}$ and $b = \max\{t : \omega_t > 0\}$ denote the occasions of the first
 175 and last captures, and $I(\cdot)$ is the indicator function. The model is parameterized in
 176 terms of:

- 177 1) **Recruitment rates:** the number of individuals that enter the population between
 178 occasions t and $t + 1$ per individual present on occasion t (γ_t), $t = 1, \dots, T - 1$,
- 179 2) **Survival probabilities:** the probability that an individual present on occasion t
 180 is also present on occasion $t + 1$ (ϕ_t), $t = 1, \dots, T - 1$,
- 181 3) **Capture probabilities:** the probability that an individual present on occasion t
 182 is encountered once or more (p_t), $t = 1, \dots, T$, and
- 183 4) **Event probabilities:** the conditional probability of event E given that an indi-
 184 vidual is encountered (ρ_E), $E \in \{L, R, S, B\}$.

185 The derived parameter $\xi(a|\boldsymbol{\gamma}, \boldsymbol{\phi}, \boldsymbol{p})$ models the probability that an individual is first
 186 captured on occasion a given that it is captured at least one time, and $\chi(b|\boldsymbol{\phi}, \boldsymbol{p})$
 187 models the probability that an individual released on occasion b is not recaptured.
 188 Expressions for these parameters are provided in Appendix A.1. Prior distributions
 189 for the model parameters were chosen to be non-informative whenever possible and
 190 are described in Appendix A.2.

191 3.2 Inference

192 As Link et al. (2010) explains, maximum likelihood (ML) methods are hard to imple-
 193 ment for the LMM. Although the likelihood function can be written down easily, it is
 194 difficult to compute. The distribution of \boldsymbol{f} given N and $\boldsymbol{\theta}$ is a mixture of multinomial
 195 distributions, and its density is easily formulated by summing over all possible values
 196 of \boldsymbol{x} that satisfy the latent vector constraint. Explicitly:

$$L(\boldsymbol{\theta}, N|\boldsymbol{f}) = \sum_{\{\boldsymbol{x}:\boldsymbol{A}'\boldsymbol{x}=\boldsymbol{f}\}} f(\boldsymbol{x}|N, \boldsymbol{\theta}).$$

197 However, there may be many values of \boldsymbol{x} that satisfy these constraints (even for
 198 fixed N), and there is no simple way to identify them all. This makes it difficult
 199 to compute the sum directly and to apply ML inference. Instead, Link et al. (2010)
 200 applies Bayesian inference treating \boldsymbol{x} as missing data and working with the joint
 201 posterior distribution of \boldsymbol{x} , N , and $\boldsymbol{\theta}$ given \boldsymbol{f} :

$$\pi(\boldsymbol{x}, N, \boldsymbol{\theta}|\boldsymbol{f}) \propto I(\boldsymbol{f} = \boldsymbol{A}'\boldsymbol{x})f(\boldsymbol{x}|N, \boldsymbol{\theta})\pi(N, \boldsymbol{\theta}). \quad (1)$$

202 Inference is then obtained by sampling from this distribution via MCMC.

203 The MCMC algorithm that Link et al. (2010) presents is a variant of the Metropolis-

204 within-Gibb's algorithm which alternately updates the values of $\boldsymbol{\theta}$ and \boldsymbol{x} (note that
 205 N is fully defined by \boldsymbol{x} and is treated as a derived parameter in the missing data
 206 approach). Updating the value of $\boldsymbol{\theta}$ given \boldsymbol{x} is equivalent to a single MCMC iteration
 207 for the parameters of the underlying mark-recapture model and can be performed
 208 with standard methods. However, it is challenging to update \boldsymbol{x} given $\boldsymbol{\theta}$ in an effi-
 209 cient way. If proposals are generated by making simple changes to \boldsymbol{x} , e.g. adding
 210 or subtracting from randomly selected elements, then they are unlikely to satisfy the
 211 latent vector constraint and will almost always be rejected. To avoid this problem,
 212 Link et al. (2010) suggests an algorithm that uses vectors from the null space of \mathbf{A}'
 213 to generate proposals for \boldsymbol{x} that always satisfy the latent vector constraint. Suppose
 214 that $\mathbf{b}_1, \dots, \mathbf{b}_R$ form a basis of $\text{null}(\mathbf{A}')$. Given the current values of $\boldsymbol{\theta}$, \boldsymbol{x} , and N ,
 215 call them $\boldsymbol{\theta}^{curr}$, \boldsymbol{x}^{curr} and N^{curr} , the algorithm updates \boldsymbol{x} and N by repeating the
 216 following two substeps for each $r = 1, \dots, R$:

217 1) Generate proposals \boldsymbol{x}^{prop} and N^{prop} by:

218 i) sampling c_r from the discrete uniform distribution on $-D_r, \dots, -1, 1, D_r$,

219 ii) setting $\boldsymbol{x}^{prop} = \boldsymbol{x}^{curr} + c_r \mathbf{b}_r$, and

220 iii) defining $N^{prop} = \sum_{r=1}^K x_r^{prop}$.

221 2) Compute the Metropolis-Hastings ratio:

$$\alpha(\boldsymbol{x}^{curr}, N^{curr}; \boldsymbol{x}^{prop}, N^{prop}) = \min \left\{ 1, \frac{f(\boldsymbol{x}^{prop} | N^{prop}, \boldsymbol{\theta}^{curr}) \pi(N^{prop}, \boldsymbol{\theta}^{curr})}{f(\boldsymbol{x}^{curr} | N^{curr}, \boldsymbol{\theta}^{curr}) \pi(N^{curr}, \boldsymbol{\theta}^{curr})} \right\}$$

222 and accept the proposals with probability $\alpha(\boldsymbol{x}^{curr}, \boldsymbol{x}^{prop})$.

223 The key to this algorithm is that $\mathbf{A}'\mathbf{b}_r = 0$ for each $r = 1, \dots, R$ so that $\mathbf{A}'\boldsymbol{x}^{prop} =$
 224 $\mathbf{A}'\boldsymbol{x}^{curr} + c_r \mathbf{A}'\mathbf{b}_r = \mathbf{f}$. This means that \boldsymbol{x}^{prop} always satisfies the latent vector con-

225 straint (provided that \boldsymbol{x}^{curr} also satisfies the constraint). The values $D_r \in Z$ are
226 tuning parameters that need to be chosen interactively or before starting the chain.

227 Although this algorithm solves the problem of generating valid proposals for \boldsymbol{x} and
228 N , the computational cost grows exponentially with T . The dimension of $\text{null}(\boldsymbol{A}')$
229 in the genetic misidentification problem considered by Link et al. (2010) is $R =$
230 $3^T - (2^T - 1)$. Each update of \boldsymbol{x} requires 212 substeps if $T = 5$, 58,026 substeps if
231 $T = 10$, and 3.5×10^9 substeps if $T = 20$.

232 The amount of computation grows even faster for the problem of multiple marks.
233 Our model allows for $K = 5^T - 1$ possible true histories and $L = (5^T - 1) - (4^T - 1) +$
234 $2(2^T - 1)$ observable histories; the dimension of $\text{null}(\boldsymbol{A}')$ is $r = (4^T - 1) - 2(2^T - 1)$.
235 When $T = 8$, there are 390,624 possible true histories of which 325,599 are observable.
236 The MCMC algorithm of Link et al. (2010) would require 65,025 substeps for each
237 update of \boldsymbol{x} .

238 To show how the algorithm can be simplified we consider a toy example. Suppose
239 that $T = 8$ and that only the six histories shown in the top of Table 1 are observed.
240 These include two left-only, two right-only, and two simultaneous histories. Although
241 there are 390,624 possible true histories with $T = 8$ entries, the vast majority of
242 these are not compatible with the observed histories. In this example, only ten true
243 histories are compatible with the observed data. These include the six observed
244 histories plus the four extra histories formed by combining each left-only and each
245 right-only history, shown in the bottom of Table 1. Any other true history would
246 have produced an observed history not seen in the data.

247 [Table 1 about here.]

248 Modeling can now be conducted using only the six histories observed and the
249 ten compatible true histories. Redefine \boldsymbol{f} to be the vector of length 6 containing

250 counts for the observed histories and \mathbf{x} the vector of length 10 containing counts for
 251 the compatible true histories. The latent vector constraints between \mathbf{f} and \mathbf{x} are
 252 determined by pairing each parent in the observed histories with its children in the
 253 compatible true histories. Specifically, the number of times a parent is observed must
 254 equal the sum of the counts from all of its children in the compatible true histories.
 255 In the toy example, the first observed history is a parent of the 1st, 7th, and 9th
 256 compatible true histories. The corresponding constraint is $f_1 = x_1 + x_7 + x_9$. The
 257 remaining constraints are: $f_2 = x_2 + x_8 + x_{10}$, $f_3 = x_3 + x_7 + x_8$, $f_4 = x_4 + x_9 + x_{10}$,
 258 $f_5 = x_5$, and $f_6 = x_6$. One consequence is that \mathbf{x} has only four free elements.
 259 New values of \mathbf{x} can be sampled by updating only x_7, \dots, x_{10} in turn and adjusting
 260 the remaining counts accordingly. Further, the values of x_7, \dots, x_{10} are bounded by
 261 the observed counts. In the example, $0 \leq x_7 \leq \min(f_1, f_3)$, $0 \leq x_8 \leq \min(f_2, f_3)$,
 262 $0 \leq x_9 \leq \min(f_1, f_4)$ and $0 \leq x_{10} \leq \min(f_2, f_4)$. These bounds can be used to define
 263 proposal distributions that are free of tuning parameters.

264 Generally, let L' denote the number of unique histories observed and K' the
 265 number of compatible true histories. Explicitly, $L' = L'_L + L'_R + L'_S$ and $K' = L' + L'_L L'_R$
 266 where L'_L , L'_R , and L'_S denote the numbers of left-only, right-only, and simultaneous
 267 histories observed. To describe the algorithm we need to know the order of the counts
 268 in \mathbf{f} and \mathbf{x} . We order \mathbf{f} so that the L'_L counts of the left-only histories come first,
 269 followed by the L'_R counts for the right-only histories, and finally by the L'_S counts for
 270 the simultaneous histories. We order \mathbf{x} in the same way with the counts for the $L'_L L'_R$
 271 extra, compatible true histories added at the end. For each of the extra histories let
 272 $l(k)$ and $r(k)$ be the indices of its left and right parents. In the toy example, $l(7) = 1$
 273 and $r(7) = 3$. The latent vector constraints are then given by the constraints on the

274 left-only histories:

$$f_j = x_j + \sum_{\{k:l(k)=j\}} x_k, \quad j = 1, \dots, L'_L,$$

275 the constraints on the right-only histories:

$$f_j = x_j + \sum_{\{k:r(k)=j\}} x_k, \quad j = L'_L + 1, \dots, L'_L + L'_R,$$

276 and the constraints on the simultaneous histories:

$$f_j = x_j, \quad j = L'_L + L'_R + 1, \dots, L'.$$

277 These equations show that \mathbf{x} is completely defined by the $L'_L L'_R$ elements $x_{L'+1}, \dots, x_{K'}$
 278 and that $x_k \leq \min(f_{l(k)}, f_{r(k)})$ for each $k = L' + 1, \dots, K'$.

279 Updates to \mathbf{x}^{curr} given $\boldsymbol{\theta}^{curr}$ can then be performed with the following algorithm.

280 For each $k = L' + 1, \dots, K'$:

281 1) Generate proposals \mathbf{x}^{prop} and N^{prop} by:

282 i) setting $\mathbf{x}^{prop} = \mathbf{x}^{curr}$,

283 ii) sampling x_k^{prop} from $\{0, \dots, \min(f_{l(k)}, f_{r(k)})\}$,

284 iii) setting $x_{l(k)}^{prop} = x_{l(k)}^{curr} - (x_k^{prop} - x_k^{curr})$ and $x_{r(k)}^{prop} = x_{r(k)}^{curr} - (x_k^{prop} - x_k^{curr})$,

285 iv) and defining $N^{prop} = \sum_{k=1}^{K'} x_k^{prop}$.

286 2) Reject the proposals immediately if $x_{l(k)}^{prop} < 0$ or $x_{r(k)}^{prop} < 0$.

287 3) Otherwise, compute the Metropolis-Hastings ratio:

$$\alpha(\mathbf{x}^{curr}, \mathbf{x}^{prop}) = \min \left\{ 1, \frac{f(\mathbf{x}^{prop} | N^{prop}, \boldsymbol{\theta}^{curr}) \pi(N^{prop}, \boldsymbol{\theta}^{curr})}{f(\mathbf{x}^{curr} | N^{curr}, \boldsymbol{\theta}^{curr}) \pi(N^{curr}, \boldsymbol{\theta}^{curr})} \right\}$$

288 and accept \mathbf{x}^{prop} and N^{prop} with probability $\alpha(\mathbf{x}^{curr}, \mathbf{x}^{prop})$

289 The advantage of this algorithm is that it uses only $L'_L L'_R$ steps to update \mathbf{x} . For
290 the toy example with 6 observed histories, \mathbf{x} can be updated in 4 steps. For the 2008
291 ECOCEAN whale shark data, $L'_L = 27$ and $L'_R = 24$ so the new algorithm requires
292 only 648 substeps to update \mathbf{x} . This is much smaller than the 65,025 substeps required
293 by the algorithm of Link et al. (2010).

294 We have implemented the MCMC sampling algorithm for fitting the multiple
295 MARK model directly in R and using the JAGS interpreter for the BUGS language
296 (Plummer, 2003, 2011; Team, 2012). An R package providing functions to format
297 the data and to fit these models is available from the website of the first author at
298 www.simon.bonniers.ca/MultiMark. In application to the 2008 ECOCEAN whale
299 shark data, we ran three parallel chains with 10,000 burn-in iterations and 50,000
300 sampling iterations each. Convergence was monitored with the Gelman-Rubin-Brooks
301 (GRB) diagnostic (Brooks and Gelman, 1998) as implemented in the R package CODA
302 (Plummer et al., 2006).

303 4 Simulation Study

304 To assess the performance of the model presented in the previous section we conducted
305 simulation studies under a variety of scenarios. Here we present the results from two
306 simulation scenarios which illustrate our main results.

307 In our simulations, we compared the performance of the new model (the two-

308 sided model) with two alternatives. First, we fit models using considering only the
 309 data from the left-side photographs (the one-sided model). Capture histories were
 310 constructed by combining all events that include a left-side photograph, namely L,
 311 S, and B, ignoring all right-side photographs. The models we fit to this data were
 312 equivalent to the LBJS model with prior distributions as given in Appendix A.2.
 313 Second, we fit a Bayesian method of combining inferences from the two sides under
 314 the assumption of independence as in (Wilson et al., 1999) (combined inference). To
 315 do this, we fit separate models to the data from the left- and right-side photographs
 316 and averaged the values drawn on each iteration of the separate MCMC samplers
 317 prior to computing summary statistics. For example, let $\phi_t^{(k,L)}$ and $\phi_t^{(k,R)}$ represent
 318 the values of ϕ_t drawn on the k^{th} iterations of the MCMC samplers run separately
 319 for models of the the left- and right-side data. Let $\widehat{\text{Var}}^{(L)}(\phi_t)$ and $\widehat{\text{Var}}^{(R)}(\phi_t)$ be
 320 the posterior variances estimated from all iterations. Combined inference for ϕ_t was
 321 obtained by computing the inverse variance weighted average of $\phi_t^{(k,L)}$ and $\phi_t^{(k,R)}$

$$\phi_t^{(k)} = \frac{(\widehat{\text{Var}}^{(R)}(\phi_t)\phi_t^{(k,L)} + \widehat{\text{Var}}^{(L)}(\phi_t)\phi_t^{(k,R)})}{\widehat{\text{Var}}^{(L)}(\phi_t) + \widehat{\text{Var}}^{(R)}(\phi_t)}$$

322 and then computing summary statistics from the new chain $\phi_t^{(1)}, \phi_t^{(2)}, \dots$. Credible
 323 intervals can then be computed directly from the new chain without relying on normal
 324 approximations. The mean of the values in the new chain is exactly equal to the
 325 inverse-variance weighted average of means from the separate chains.

326 We expected that the new model would provide better inference than the two
 327 alternatives. In particular, we expected that credible intervals from the one-sided
 328 models would be wider than the corresponding intervals from the two-sided model.
 329 We also expected that credible intervals produced by combined inference would be
 330 narrower than the intervals from the two-sided model but would not achieve the

331 nominal coverage probability.

332 In the first scenario, we generated data under the assumption that all events were
333 equally likely given capture ($\rho_L = \rho_R = \rho_B = \rho_S = .25$). We set $T = 10$ and
334 generated data by simulating true capture histories sequentially until 200 observed
335 capture histories were produced (each true history contributing either 0, 1, or 2
336 histories to the observed data). Demographic parameters were simulated from the
337 distributions:

$$\text{logit}(\phi_t) \sim N(\text{logit}(.80), .30), \quad \text{logit}(p_t) \sim N(\text{logit}(.80), .30), \quad \log(\gamma_t) \sim N(\log(.25), .30).$$

338 A total of 100 data sets were simulated and analyzed. The median number of true his-
339 tories simulated before 200 observed histories were obtained was 164 (min=150,max=180),
340 the median number of unique individuals observed was 138 (min=127,max=148), and
341 the median number of captures per individual was 2 (min=1,max=10).

342 Table 2 presents statistics comparing the mean-squared error (MSE) of the pos-
343 terior means and the mean width and estimated coverage probability of the 95%
344 credible intervals obtained from the alternative models. The MSE of the two-sided
345 model and the combined-inference were similar for all parameters and smaller than
346 those of the one-sided model by between 10% and 25%. Credible intervals for both
347 the one-sided and two-sided models achieved the nominal coverage rate for all param-
348 eters, but the credible intervals for the one-sided model were wider by approximately
349 10%. In comparison, the credible intervals from the combined inference were narrower
350 than those of the two-sided model by 20% or more but failed to achieve the nominal
351 coverage rate.

352 In the second scenario, we simulated data from the same model except that both
353 marks were seen with probability one each time an individual was captured ($\rho_S = 1$).

354 This represents the extreme situation in which there is complete dependence between
355 the two marks and no uncertainty in the true capture histories. In this case, the one-
356 sided and two-sided models produce identical results. The median number of histories
357 simulated in the 100 data sets before 200 observed histories were obtained was 215
358 (min=204,max=227) and the median number of captures per observed individual was
359 2 (min=1,max=10).

360 Point estimates produced by the two models in this scenario were almost exactly
361 equal and the MSE of the two models was indistinguishable (see Table 2). However,
362 there were clear differences in the interval estimates. While the intervals produced by
363 combined-inference were, on average, 30% narrower, the coverage of these intervals
364 was well below the nominal value.

365 [Table 2 about here.]

366 5 Results

367 The data provided in the ECOCEAN whale shark library contained a total of 96
368 observed encounter histories for the 2008 study period. Of these, 27 histories (28%)
369 were constructed from left-side photographs alone, 24 (25%) were constructed from
370 right-side photographs alone, and 45 (47%) contained at least one encounter with
371 photographs taken from both sides simultaneously. Along with the model presented
372 in Section 3, we computed inferences for \mathbf{p} , \mathbf{f} , and ϕ from the alternative models
373 described in Section 4.

374 Table 3 provides posterior summary statistics for the LBJs parameters model
375 obtained from the two-sided model. Inferences about all parameters are relatively
376 imprecise because of the relatively small number of individuals captured and the low
377 capture probabilities, but the posterior means follow the expected patterns. Point

378 estimates for the survival probability (the probability that a whale shark remains at
379 NMP between occasions) are at or above .90 in the first two periods, below .70 in the
380 last two periods, and about .80 in between. The posterior mean recruitment rate is
381 very high in week two, suggesting that most of the sharks entered during this period,
382 and lower thereafter. This table also provides summary statistics for the population
383 growth rate, $\lambda_k = \phi_k + f_k$, $k = 1, \dots, K - 1$, computed as a derived parameter.
384 Although the 95% credible intervals for λ_k cover 1.00 for all k , the point estimates
385 are greater than 1.00 for the first two periods, close to 1.00 in the next three periods,
386 and less than .75 in the last two periods. This suggests that the aggregation of whale
387 sharks grew during the first two periods, remained almost steady during the next three
388 periods, and declined during the last two periods. This supports the hypothesis that
389 whale sharks aggregate at NMP to feed after the major coral spawn which occurred
390 between April 9 and 12 in 2008 (Chalmers, 2008, pg. 33).

391 [Table 3 about here.]

392 Table 4 provides posterior summary statistics for the conditional event probabil-
393 ities. These results show that sharks were photographed from both sides simultane-
394 ously most often ($\hat{\rho}_S = .45(.36, .54)$) and that the probabilities that an individual was
395 photographed from either the left or right side only were similar ($\hat{\rho}_L = .29(.20, .38)$
396 versus $\hat{\rho}_R = .21(.13, .29)$).

397 The posterior mean of N , the number of unique sharks encountered during the
398 2008 season, was 88 with 95% credible interval (82,93). The full posterior distribution
399 of N is shown in Figure 1 and compared with the prior distribution of N generated by
400 simulating data sets from the prior predictive distribution conditional on there being
401 96 observed capture histories and at least 72 true histories (the minimum number
402 given that 24 of 96 observed histories included right-side photographs alone). Whereas

403 the prior distribution of N is close to uniform, the posterior distribution is strongly
404 peaked and concentrates 95% of its mass between 82 and 93. We conclude that
405 between 3 (3.1%) and 14 (14.6%) of the sharks encountered during the 2008 season
406 were photographed from both the left and right sides on separate occasions without
407 ever being matched.

408 [Table 4 about here.]

409 [Figure 1 about here.]

410 Comparisons of the three chains starting from different initial values provided
411 no evidence of convergence problems. Traceplots all indicated that the three chains
412 converged within the burn-in period, GRB diagnostic values were all less than 1.02,
413 and the estimated MCMC error was less than 2.6% of the posterior standard deviation
414 for each parameter. Based on these results, we are confident that the chains were long
415 enough to produce reliable summary statistics.

416 The plots in Figure 2 compare inferences for the survival, recruitment, and growth
417 rates from the four alternative models. Posterior means from the four models are all
418 very similar and the 95% credible intervals for all parameters overlap considerably.
419 Comparison of the widths of the 95% credible intervals from the left- and right-side
420 data alone showed that the two-sided model provided improved inference for most,
421 but not all, parameters. On average, the 95% credible intervals for the recruitment
422 rates produced by the two-sided model were 93% and 69% as wide as those produced
423 from the left- and right-side data alone. The 95% credible intervals for the survival
424 probabilities produced by the two-sided model were 78% as wide as those from the
425 right-side data, on average, but 103% as wide as those from the left-side data. This
426 last result seems to be caused by issues with the upper bound on the survival prob-
427 abilities as the 95% credible intervals for the logit transformed survival probabilities

428 produced from the two-sided model were, on average, 90% and 89% as wide as those
429 obtained from the left- and right-side data alone. Credible intervals produced via
430 combined inference were on average 12% smaller than those obtained from the two-
431 sided model; however, based on the results in the previous section, we believe that
432 these intervals would not achieve the nominal coverage rate and do not reflect the
433 variability of the parameters correctly.

434 [Figure 2 about here.]

435 **6 Conclusion**

436 The simulation results presented in Section 4 illustrate the main advantages of our
437 model over the previous approaches to analyzing mark-recapture data with multiple,
438 non-invasive marks. In general, estimates from our model will be more precise than
439 estimates based on only one mark. In contrast, the apparent gain in precision from
440 combining estimators computed separately for each mark under the assumption of in-
441 dependence is artificial and credible/confidence intervals computed by these methods
442 will not achieve the nominal coverage rate. The effect is strongest when the probab-
443 ility that both marks are seen simultaneously is high and the separate estimators are
444 highly dependent.

445 The disadvantage of combining data from multiple marks is that the model is
446 more complex and computations take longer. A single chain of 60,000 iterations for
447 the 2008 whale shark data implemented in native R code ran in 28.6 minutes on a
448 Linux machine with a clock speed of 2.8 GHz. In comparison, a chain of the same
449 length for the one-sided data finished in 6.2 minutes. Our algorithm is less complex
450 than that of Link et al. (2010), but the amount of computation is still proportional
451 to the square of the number of observed histories and the chains may take too long to

452 run for some large data sets. We are exploring possible solutions including developing
453 more efficient methods of computation and approximating the posterior distribution.

454 Although we have described our model for two marks, it can easily be extended for
455 data with any number of marks. We expect that including more marks will strengthen
456 differences between our model, the one-sided model, and combined inference seen in
457 the simulation study. The model can also be adapted easily to estimate the size of
458 an open population. Following Link et al. (2010), one can include the null encounter
459 history (vector of 0s) in the set of possible true histories. Then \boldsymbol{x} would have length
460 $K' = L' + L'_L L'_R + 1$ and $N = \sum_{k=1}^{K'} x_k$ would denote the total population size. Because
461 the observed histories do not restrict the number of individuals never encountered
462 the constraints on \boldsymbol{x} would not change. The only differences are that the MCMC
463 algorithm presented in Section 3.2 would require one more substep to update the
464 number of individuals never encountered and that the prior bound on N must be
465 increased to allow for the unobserved individuals.

466 Non-invasive marks are especially useful for mark-recapture studies that rely on
467 public data collection because they can often be observed without special equipment
468 or physical interaction. So called citizen science projects involving “public partici-
469 pation in organized research efforts” (Dickinson and Bonney, 2012, pg. 1) play an
470 important role in ecological monitoring. Large teams of volunteer researchers can
471 cover large geographical areas and quickly collect large data sets. As examples of
472 successful, large scale, citizen science projects in the United States, Dickinson and
473 Bonney (2012) highlights the US Geological Survey’s North American Breeding Bird
474 Survey (BBS), the National Audubon Society’s Christmas Bird Count, and projects
475 of The Cornell Lab of Ornithology at Cornell University. The authors estimate that
476 “200,000 people participate in [their] suite of bird monitoring projects each year”
477 (Dickinson and Bonney, 2012, pg. 10).

478 One concern with many citizen science projects is the reliability of the data.
479 Some general issues concerning the accuracy and analysis of data from citizen science
480 projects are discussed by Cooper et al. (2012). Though the ECOCEAN library does
481 rely on reports from untrained observers, it differs from similar projects in that citizens
482 provide no more than the raw data. Most importantly, the contributors do not identify
483 the sharks they photograph. Instead, the submit their photographs to the library and
484 matches suggested by the paired computer algorithms are all confirmed by trained
485 researchers (see Section 2). Hence, the data does not depend on the ability of tourists
486 or tour operators to identify spot patterns and matches can be reconfirmed at any
487 time. Even the reported times that a photograph was taken can be confirmed from
488 the digital timestamp. For these reasons, we are confident that errors in the data set
489 are minimized and that the results provided in Section 5 accurately reflect the arrival
490 and departure of sharks from NMP in 2008.

491 Although we are confident in our results, some of the assumptions of our model
492 given in Section 3 may oversimplify the population’s dynamics. Sharks may move
493 temporarily to other areas of the reef and factors like age, sex, or fitness might affect
494 the length of time that a shark remains at NMP. The objective of this research was
495 to develop and illustrate a general method for modeling data with multiple marks,
496 and we intend to explore more complicated models of the ECOCEAN data in further
497 work. Changes in survival, fecundity, and capture over time or among individuals
498 might be accounted for with covariates or random effects, and temporary emigration
499 might be modeled with Pollock’s robust design (Pollock, 1982). We also intend to
500 model data from multiple years in order to assess changes in the population over time.

Acknowledgments

We thank Laura Cowen for providing comments on a previous draft of the manuscript. Matt Schofield also commented on drafts and provide valuable discussions during the development of our model. Support for this work was provided in part by the NSF-Kentucky EPSCOR Grant (NSF Grant No. 0814194). We are aware that similar methods for analyzing data with multiple marks are being developed by Brett McClintock and Paul Conn and by Rachel Fewster, and recommend that our work be cited together.

References

- Arzoumanian, Z., Holmberg, J., and Norman, B. (2005). An astronomical pattern-matching algorithm for computer-aided identification of whale sharks rhincodon typus. *Journal of Applied Ecology* **42**, 999–1011.
- Bonner, S. J. (2013). Response to: A new method for estimating animal abundance with two sources of data in capture-recapture studies. *Methods in Ecology and Evolution* In press.
- Brooks, S. P. and Gelman, A. E. (1998). General methods for monitoring convergence of iterative simulations. *Journal of Computational and Graphical Statistics* **7**, 434–455.
- Chalmers, A. (2008). *Temporal and spatial variability in coral condition at Sandy Bay, Ningaloo*. PhD thesis, The University of Western Australia.
- Cooper, C. B., Hochachka, W. M., and Dhondt, A. A. (2012). The opportunities and challenges of citizen science as a tool for ecological research. In Dickinson, J. L.

- 523 and Bonney, R., editors, *Citizen Science: Public Participation in Environmental*
524 *Research*, pages 99–113. Comstock Pub. Associates.
- 525 Da-Silva, C. Q. (2006). Asymptotics for a population size estimator of a partially
526 uncatchable population. *Annals of the Institute of Statistical Mathematics* **59**,
527 603–615.
- 528 Da-Silva, C. Q., Rodrigues, J., Leite, J. G., and Milan, L. A. (2003). Bayesian es-
529 timation of the size of a closed population using photo-id data with part of the
530 population uncatchable. *Communications in Statistics - Simulation and Computa-*
531 *tion* **32**, 677–696.
- 532 Dickinson, J. L. and Bonney, R. (2012). Why citizen science? In Dickinson, J. L.
533 and Bonney, R., editors, *Citizen Science: Public Participation in Environmental*
534 *Research*, pages 1–14. Comstock Pub. Associates.
- 535 Holmberg, J., Norman, B., and Arzoumanian, Z. (2009). Estimating population size,
536 structure, and residency time for whale sharks *rhincodon typus* through collabora-
537 tive photo-identification. *Endangered Species Research* **7**, 39–53.
- 538 Link, W. A. and Barker, R. J. (2005). Modeling association among demographic
539 parameters in analysis of open population capture-recapture data. *Biometrics* **61**,
540 46–54.
- 541 Link, W. A., Yoshizaki, J., Bailey, L. L., and Pollock, K. H. (2010). Uncovering a
542 latent multinomial: Analysis of mark-recapture data with misidentification. *Bio-*
543 *metrics* **66**, 178–185.
- 544 Lukacs, P. M. and Burnham, K. P. (2005). Estimating population size from DNA-

- 545 based closed capture-recapture data incorporating genotyping error. *Journal of*
546 *Wildlife Management* **69**, 396–403.
- 547 Madon, B., Gimenez, O., McArdle, B., Scott Baker, C., and Garrigue, C. (2011). A
548 new method for estimating animal abundance with two sources of data in capture-
549 recapture studies. *Methods in Ecology and Evolution* **2**, 390–400.
- 550 McClintock, B. T., Conn, P., Alonso, R., and Crooks, K. R. (2013). Integrated
551 modeling of bilateral photo-identification data in mark-recapture analyses. *Ecology*
552 In press.
- 553 Plummer, M. (2003). JAGS: A program for analysis of Bayesian graphical mod-
554 els using Gibbs sampling. In *Proceedings of the 3rd International Workshop on*
555 *Distributed Statistical Computing (DSC 2003)*, pages 1–10, Vienna, Austria.
- 556 Plummer, M. (2011). *rjags: Bayesian graphical models using MCMC*. R package
557 version 3-5.
- 558 Plummer, M., Best, N., Cowles, K., and Vines, K. (2006). CODA: Convergence
559 diagnosis and output analysis for MCMC. *R News* **6**, 7–11.
- 560 Pollock, K. H. (1982). A Capture-Recapture Design Robust to Unequal Probability
561 of Capture. *The Journal of Wildlife Management* **46**, 752–757.
- 562 Team, R. D. C. (2012). *R: A Language and Environment for Statistical Computing*.
563 R Foundation for Statistical Computing, Vienna, Austria. ISBN 3-900051-07-0.
- 564 Van Tienhoven, A., Den Hartog, J., Reijns, R., and Peddemors, V. (2007). A
565 computer-aided program for pattern-matching of natural marks on the spotted
566 raggedtooth shark *carcharias taurus*. *Journal of Applied Ecology* **44**, 273–280.

567 Wilson, B., Hammond, P. S., and Thompson, P. M. (1999). Estimating size and
568 assessing trends in a coastal bottlenose dolphin population. *Ecological Applications*
569 **9**, 288–300.

570 Wright, J. A., Barker, R. J., Schofield, M. R., Frantz, A. C., Byrom, A. E., and
571 Gleeson, D. M. (2009). Incorporating genotype uncertainty into mark-recapture-
572 type models for estimating abundance using DNA samples. *Biometrics* **65**, 833–40.

573 Yoshizaki, J., Brownie, C., Pollock, K. H., and Link, W. A. (2011). Modeling misiden-
574 tification errors that result from use of genetic tags in capture-recapture studies.
575 *Environmental and Ecological Statistics* **18**, 27–55.

576 Yoshizaki, J., Pollock, K. H., Brownie, C., and Webster, A. (2009). Modeling misiden-
577 tification errors in capture-recapture studies using photographic identification of
578 evolving marks. *Ecology* **90**, 3–9.

579 **A**

580 **A.1 Derived Parameters**

581 As in Link and Barker (2005):

$$\xi(a|\gamma, \phi, \mathbf{p}) = \frac{\kappa_a}{\sum_{t=1}^T \kappa_t}$$

582 where:

$$\begin{aligned}\kappa_1 &= p_1 \\ \kappa_2 &= (\phi_1(1 - p_1) + \gamma_1)p_2 \\ \kappa_{t+1} &= p_{t+1} \left(\frac{\kappa_t(1 - p_t)\phi_t}{p_t} + \gamma_t \prod_{k=1}^{t-1} (\phi_k + \gamma_k) \right), \quad t = 2, \dots, T - 1.\end{aligned}$$

583 Similarly:

$$\chi(t|\boldsymbol{\phi}, \mathbf{p}) = (1 - \phi_t) + \phi_t(1 - p_{t+1})\chi(t + 1|\boldsymbol{\phi}, \mathbf{p}), \quad t = 1, \dots, T - 1$$

584 with $\chi(T|\boldsymbol{\phi}, \mathbf{p}) = 1$.

585 A.2 Prior Distributions

586 Parameters in the model of the true histories were assigned the following prior distri-
587 butions:

$$\begin{aligned}\text{logit}(\phi_t) &\sim N(\mu_\phi, \sigma_\phi^2), \quad t = 1, \dots, T - 1 \\ \text{logit}(p_t) &\sim N(\mu_p, \sigma_p^2), \quad t = 1, \dots, T \\ \log(\gamma_t) &\sim N(\mu_\gamma, \sigma_\gamma^2), \quad t = 1, \dots, T - 1 \\ (\rho_L, \rho_R, \rho_S, \rho_B) &\sim \text{Dirichlet}((1, 1, 1, 1)^T) \\ N &\sim U\{0, \dots, U_{\max}\}\end{aligned}$$

588 The value U_{\max} must be bigger than the true value of N . This can be achieved by
589 setting $U_{\max} = \sum_{l=1}^L f_l$ when the model conditions on first capture.

590 Hyperparameters were assigned the prior distributions:

$$\mu_\phi, \mu_p \sim N(0, 2)$$

$$\mu_\gamma \sim N(0, .25)$$

$$\sigma_\phi, \sigma_p, \sigma_\gamma \sim HT(3, .9)$$

591 Here $HT(\nu, \sigma)$ represents the half t -distribution with ν degrees of freedom and scale
592 parameter σ . All prior distributions were assumed independent.

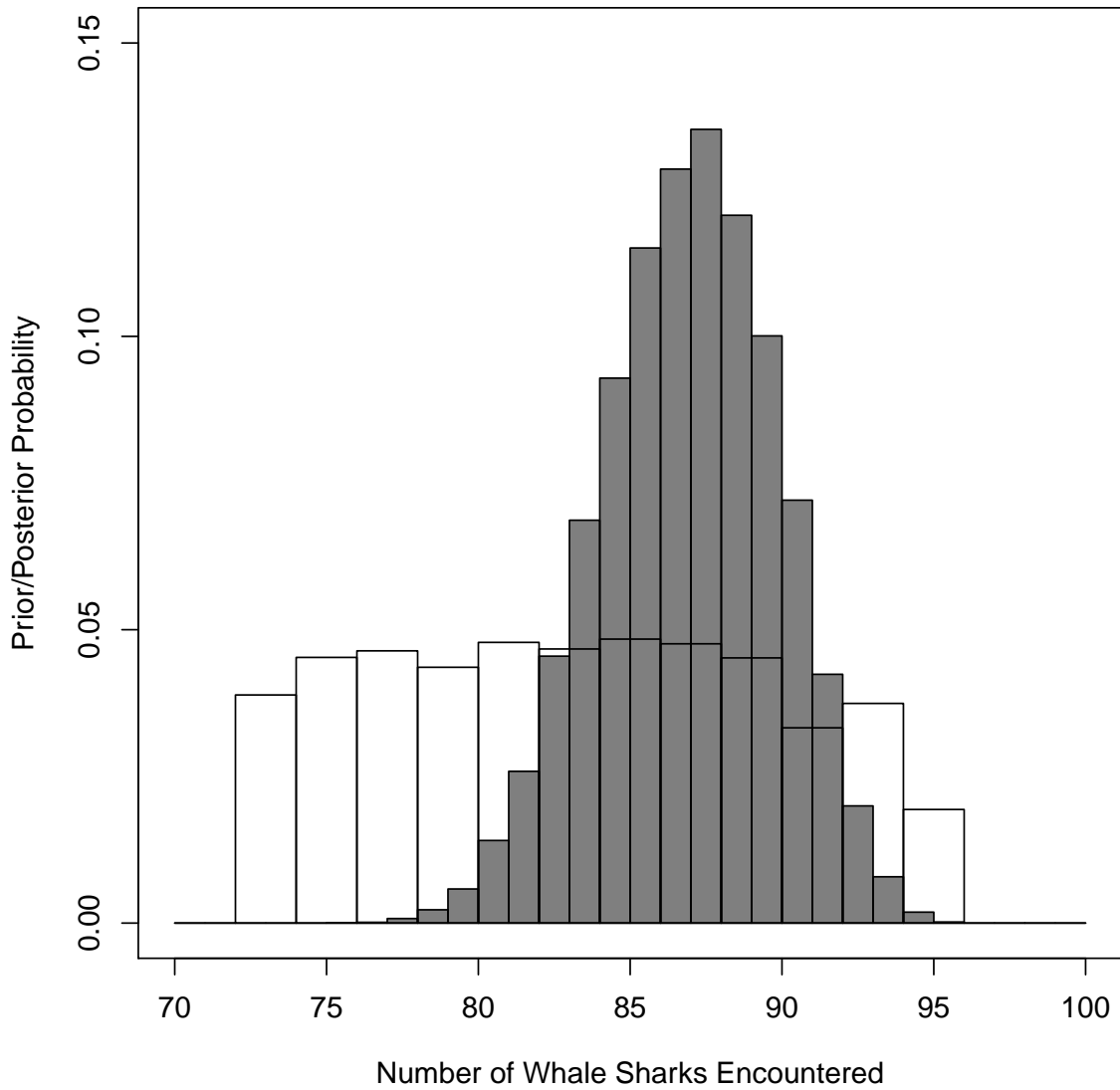


Figure 1: Comparison of the prior and posterior distribution of N . The prior distribution of N , conditional on there being 96 observed capture histories and at least 72 unique individuals, is shown by the histogram with white bars. The posterior distribution of N is shown by the histogram with grey bars.

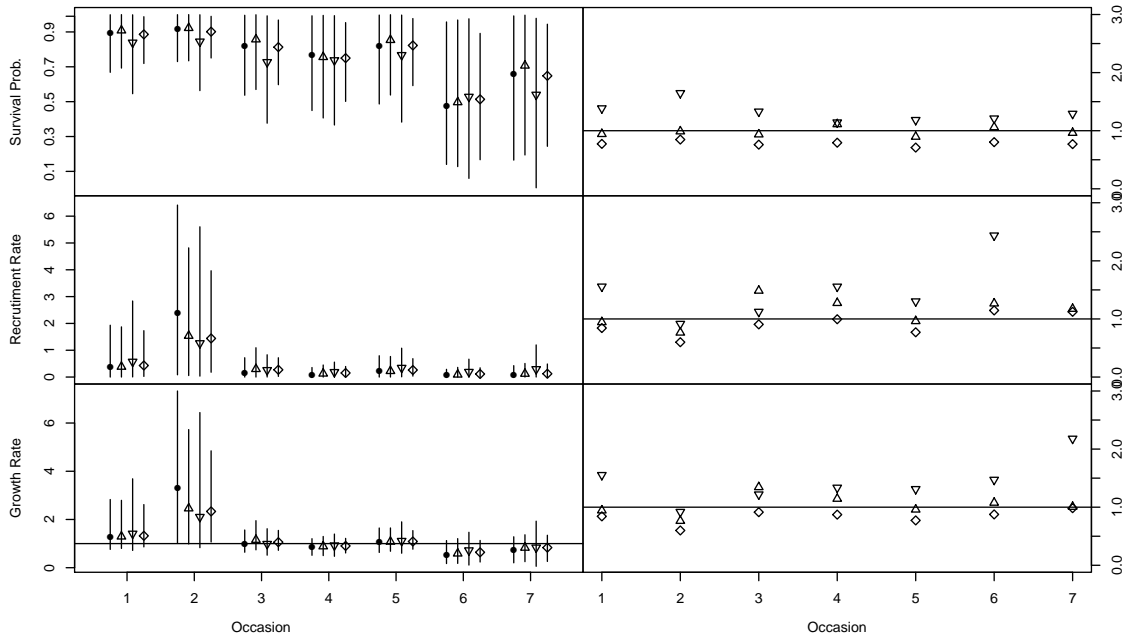


Figure 2: Comparison between the two-sided model and the three alternative models. The plots on the left-side of the figure compare the posterior means (points) and 95% credible intervals (vertical lines) of the survival probability (top), recruitment rate (middle), and population growth rate (bottom) obtained from the four models. The plots on the right side of the figure display the posterior standard deviations from the three alternative models relative to the posterior standard deviation from the two-sided model. Results from the two-sided model are represented by the circles, from the left-side photographs only by the upward pointing triangles, from the right-side photographs only by the downward pointing triangles, and from combined inference by the diamonds.

Table 1: Example of possible observed and true capture histories. Suppose that the data comprises the six observed histories given in the top of the table. The possible true histories that may have generated this data include these six plus the four additional histories in the bottom of the table.

	k	History
Observed	1	00L0L000
	2	0000L000
	3	00R00000
	4	000RR000
	5	00SBR000
	6	S0S00000
Unobserved	7	00B0L000
	8	00R0L000
	9	00LRB000
	10	000RB000

Table 2: Performance of the estimates from the two simulation scenarios. Each column of the table presents the MSE of the posterior mean relative to the MSE of the posterior mean of the one-sided model, and the median width and estimated coverage probability of the 95% credible intervals for the survival probability (ϕ), recruitment rate (f), and growth rate (λ) for one of the three models – one-sided (OS), two-sided (TS), or combined-inference (CI). The models are described in Section 4.

		Simulation 1			Simulation 2	
		OS	TS	CI	TS	CI
ϕ	MSE	1.00	.89	.87	1.00	1.00
	Width	.23	.20	.16	.17	.12
	Cover	.97	.96	.90	.95	.84
f	MSE	1.00	.88	.81	1.00	1.00
	Width	.35	.31	.24	.26	.18
	Cover	.97	.95	.90	.95	.84
λ	MSE	1.00	.88	.82	1.00	1.00
	Width	.41	.36	.29	.31	.22
	Cover	.98	.97	.95	.97	.87

Table 3: Posterior summary statistics for the demographic parameters ϕ_k , f_k , λ_k , and p_k obtained from the two-sided model. The columns of the table provide posterior means followed with equal-tailed 95% credible intervals.

Occ (k)	Survival (ϕ_k)	Recruitment (f_k)	Growth (λ_k)	Capture (p_k)
1	0.90(0.67,1.00)	0.36(0.00,1.93)	1.26(0.76,2.83)	0.23(0.08,0.43)
2	0.92(0.73,1.00)	2.40(0.08,6.41)	3.31(1.00,7.33)	0.19(0.05,0.33)
3	0.82(0.54,1.00)	0.17(0.00,0.72)	0.99(0.64,1.56)	0.26(0.15,0.43)
4	0.77(0.45,0.99)	0.09(0.00,0.36)	0.85(0.51,1.20)	0.22(0.13,0.34)
5	0.82(0.49,1.00)	0.23(0.00,0.79)	1.05(0.63,1.65)	0.22(0.12,0.36)
6	0.48(0.14,0.96)	0.06(0.00,0.29)	0.54(0.17,1.12)	0.25(0.14,0.42)
7	0.66(0.16,0.99)	0.09(0.00,0.42)	0.75(0.20,1.28)	0.20(0.06,0.37)
8	—	—	—	0.18(0.03,0.34)

Table 4: Posterior summary statistics for the conditional event probabilities.

Event (j)	Cond. Prob. (ρ_j)
1	0.29(0.20,0.38)
2	0.21(0.13,0.29)
3	0.45(0.36,0.54)
4	0.06(0.01,0.13)